CIMR RGB – Re-Gridding Toolbox

D5 - Algorithms Theoretical Baseline Document Description

Signature Page

Prepared by	Joseph Heywood, Maksym Brilenkov and Davide Decataldo	Date: 2025-04-15
Issued by	Carolina Barrack - Project Manager	Date: 2025-04-15
Approved by	ESA Technical Officer	Date:

Table of contents

Changelog

Issue	Author	Affected Section	Reason	Status	Date
1.0	S&T AS	All	Document creation	Issued	2024-11-20
1.1	S&T AS	Acronyms References 3 3.4.2, 3.4.6 3 & 4 4.7 3 4.3 4.3 Introduction 3 & 4 All sections	Updated Table RID01: MS3-MSC-1 RID15: MS3-MSC-15 RID16: MS3-MSC-16 RID17: MS3-MSC-17 RID18: MS3-MSC-18 RID20: MS3-MSC-20 RID22: MS3-MSC-22 RID24: MS3-MSC-24 RID26: MS3-MSC-26 RID01: MS3-FCA-1 RID02: MS3-FCA-2 Changed section count	Modified	2024-12-17
1.2	S&T AS	5.5.3	FM-MSC-11	Modified	2025-04-15

Acronyms

ATBD	Algorithm Theoretical Baseline Document
AMSR2	Advanced Microwave Scanning Radiometer
BG	Backus-Gilbert
BTs	Brightness Temperatures
CEA	Cylindrical Equal Area
CETB	Calibrated Passive Microwave Daily Equal-Area Scalable Earth Grid 2.0 Brightness Temperature
CG	Conjugate Gradients
CGNE	Conjugate Gradients Normal Equations
CIMR	Copernicus Imaging Microwave Radiometer
DIB	Drop-in-the-Bucket
EASE2	Equal-Area Scalable Earth 2.0
HDF	Hierarchical Data Format
ICI	Ice Cloud Imager
IDS	Inverse Distance Squared
IODD	Input/Output Data Definition
L1b, L2	Level 1b, Level 2
LW	Landweber
LAEA	Lamberts Equal Area
LTS	Long Term Support
MACRAD	Metrological Analysis of CIMR RADiometry
MRF	Measurement Response Function
MWI	Microwave Imager
NaN	Not a Number
NETCDF	Network Common Data Form
NN	Nearest Neighbour
PAD	Processing and Algorithm Development
RGB	ReGridding toolBox

RMSE	Root Mean Square Error
rSIR	Radiometer Scatterometer Image Reconstruction
SMAP	Soil Moisture Active Passive
SoW	Statement of Work
UML	Unified Modelling Language
XML	eXtensible Markup Language

1. Introduction

1.1. Purpose and Scope

This document contains the *Algorithm Theoretical Baseline Document* (ATBD) for the CIMR RGB project in accordance with the contract and the *Statement of Work* (SoW). It serves as a reference for the development, implementation, and theoretical background of the algorithms used for regridding data with the *ReGridding toolBox* (RGB). The primary purpose is to provide a detailed description of the theoretical basis and implementation strategies for each algorithm included in the toolbox, as well as their limitations and assumptions. The included algorithms can be broadly categorised into two categories: (1) the ones that do not require knowledge of antenna patterns (i.e., Nearest Neighbours, Inverse Distance Squared and Drop-in-the-Bucket) and (2) the ones that heavily rely on the knowledge of both target and source antenna patterns (i.e., Backus Gilbert inversion algorithm, radiometer Scatterometer Image Reconstruction, and gradient-based methods — Landweber and Conjugate Gradients).

1.2. Document Structure

The document is structured as follows:

- Section 1 provides an introduction and defines the scope of this document.
- Section 2 provides references.
- Section 3 describes map projections and grids used in the RGB.
- Section 4 provides a description of the regridding algorithms, including their theoretical basis, limitations, assumptions, and implementation strategies. The Section concludes with a discussion of the uncertainty propagation through the regridding algorithms.
- Section 5 discusses the implementation details related to the regridding algorithms.

2. References

2.1. Applicable Documents

AD	Title	Reference
[LI]	Request for Proposal for CIMR RGB RE-GRIDDING TOOL BOX - EXPRO - ESA RFP/3-17792/22/I-AG	Invitation letter: Request for Proposal for CIMR RGB RE-GRIDDING TOOL BOX - EXPRO Activity No. 1000035090 in the esa-star system
[SOW]	Statement of Work for “Statement of Work ESA Express Procurement - EXPRO CIMR RGB – Re-Gridding tool Box”	ESA-EOPG-EOPGMQ-SOW-48
[CC]	Draft Contract for “CIMR RGB Re-Gridding Tool Box - EXPRO”	ESA Contract No. 4000xxxxxx/22/I-AG
[TC]	Conditions of Tender for “CIMR RGB Re-Gridding Tool Box - EXPRO”	Appendix 3 EXPRO Tendering Conditions (EXPRO/TC)

2.2. Reference Documents

RD	Title	Reference
[RD1]	Numerical applications of a formalism for geophysical inverse problems	Backus GE, Gilbert JF, (1967), Numerical applications of a formalism for geophysical inverse problems. Geophys. J. R. Astron. Soc. Jul; 1967 13(1–3):247–276.
[RD2]	Global seismic tomography using Backus-Gilbert inversion.	Christophe Zaroli. Global seismic tomography using Backus-Gilbert inversion. Geophysical Journal International, Oxford University Press (OUP), 2016, 207 (2), pp.876-888.
[RD3]	Backus-Gilbert footprint matching methodology applied on MWI and ICI observations	Backus-Gilbert footprint matching methodology applied on MWI and ICI observations TR/BG/MWI-ICI Issue 1.0, Rev. 1
[RD4]	Spatial resolution enhancement of SSM/I data	D.G. Long, D.L. Daum, March 1998, IEEE Transactions on Geoscience and Remote Sensing, https://doi.org/10.1109/36.662726
[RD5]	An enhanced resolution brightness temperature product for future conical scanning microwave radiometers	F. Nunziata et al., 10 Sept. 2021, IEEE Transactions on Geoscience and Remote Sensing,

		https://doi.org/10.1109/TGRS.2021.3109376
[RD6]	Backus-Gilbert footprint matching methodology applied on MWI and ICI observations	Backus-Gilbert footprint matching methodology applied on MWI and ICI observations TR/BG/MWI-ICI Issue 1.0, Rev. 1
[RD7]	GCOM-W1 AMSR2 Level 1R Product: Dataset of Brightness Temperature Modified Using the Antenna Pattern Matching Technique	T. Maeda, Y. Taniguchi and K. Imaoka, "GCOM-W1 AMSR2 Level 1R Product: Dataset of Brightness Temperature Modified Using the Antenna Pattern Matching Technique," in IEEE Transactions on Geoscience and Remote Sensing, vol. 54, no. 2, pp. 770-782, Feb. 2016
[RD10]	Algorithm Theoretical Basis Document for AMSR-E Level2A Algorithm. Revised Nov. 3, 2000	Ashcroft, P. and F. J. Wentz, (2000), Remote Sensing Systems, Available from: https://nsidc.org/sites/nsidc.org/files/technical-references/amsr_atbd_level2a.pdf
[RD14]	SMAP L1C Radiometer Half-Orbit 36 km EASE-Grid Brightness Temperatures, Version 6	Chan, S., Njoku, E. G. & Colliander, A. (2023). SMAP L1C Radiometer Half-Orbit 36 km EASE-Grid Brightness Temperatures. (SPL1CTB, Version 6). [Data Set]. Boulder, Colorado USA. NASA National Snow and Ice Data Center Distributed Active Archive Center.
[RD15]	Algorithm Theoretical Basis Document Level 1C Radiometer Data Product	Steven Chan Eni Njoku Andreas Colliander Jet Propulsion Laboratory California Institute of Technology Pasadena, CA, Revision A, 2014
[RD16]	SMAP Enhanced L1C Radiometer Half-Orbit 9 km EASE-Grid Brightness Temperatures, Version 4	Chaubell, J., Chan, S., Dunbar, R. S., Peng, J. & Yueh, S. (2023). SMAP Enhanced L1C Radiometer Half-Orbit 9 km EASE-Grid Brightness Temperatures. (SPL1CTB_E, Version 4). [Data Set]. Boulder, Colorado USA. NASA National Snow and Ice Data Center Distributed Active Archive Center.
[RD17]	Algorithm Theoretical Basis Document SMAP L1B Enhancement Radiometer Brightness Temperature Data Product	Julian Chaubell, Jet Propulsion Laboratory, California Institute of Technology Document# D-56287 Date: Dec 14, 2016
[RD18]	SMAP Twice-Daily rSIR-Enhanced EASE-Grid 2.0 Brightness Temperatures ATBD	Mary J. Brodzik , David G. Long and Molly A. Hardman, NSIDC
[RD19]	SMAP Radiometer Twice-Daily rSIR-Enhanced EASE-Grid 2.0 Brightness Temperatures, Version 2	Brodzik, M. J., Long, D. G. & Hardman, M. A. (2021). SMAP Radiometer Twice-Daily rSIR-Enhanced EASE-Grid 2.0 Brightness Temperatures. (NSIDC-0738, Version 2). [Data Set]. Boulder, Colorado USA. NASA National Snow and Ice Data Center Distributed Active Archive Center.

[RD20]	Spatial Resolution Enhancement of Earth Observation Products Using an Acceleration Technique for Iterative Methods	F. Lenti, F. Nunziata, C. Estatico and M. Migliaccio, i*n IEEE Geoscience and Remote Sensing Letters,* vol. 12, no. 2, pp. 269-273, Feb. 2015, doi: 10.1109/LGRS.2014.2335057.
[RD21]	Optimum Image Formation for Spaceborne Microwave Radiometer Products.	D. G. Long and M. J. Brodzik, in IEEE Transactions on Geoscience and Remote Sensing, vol. 54, no. 5, pp. 2763-2779, May 2016, doi: 10.1109/TGRS.2015.2505677.
[RD22]	Enhanced-Resolution SMAP Brightness Temperature Image Products.	D. G. Long, M. J. Brodzik and M. A. Hardman, in IEEE Transactions on Geoscience and Remote Sensing, vol. 57, no. 7, pp. 4151-4163, July 2019, doi: 10.1109/TGRS.2018.2889427.
[RD23]	An iteration formula for Fredholm integral equations of the first kind	Landweber L. in Amer. J. Math. 73, 615–624, 1951
[RD24]	Comparison of Accelerated Versions of the Iterative Gradient Method to Ameliorate the Spatial Resolution of Microwave Radiometer Products.	Alparone, M.; Nunziata, F.; Estatico, C.; Migliaccio, M. *Remote Sens.* 2022, *14*, 5246. https://doi.org/10.3390/rs14205246
[RD25]	Generic IPF Interface Specifications	MMFI-GSEG-EOPG-TN-07-0003, v1.8, 2009-08-03
[RD26]	Copernicus Imaging Microwave Radiometer (CIMR) Requirements Document Version 4.0	ESA-EOPSM-CIMR-MRD-3236
[RD27]	CIMR RGB Design Document	CIMR-DD-ST-RGB-001 v1.3
[RD28]	CIMR RGB Level 1c Product Data Format Specifications	CIMR--ICD-ST-RGB-002 v1.3
[RD29]	CIMR RGB Performance Assessment Plan	CIMR-TP-ST-RGB-003 v1.2
[RD30]	CIMR RGB Input/Output Data Definition	CIMR-IODD-ST-RGB-004
[RD31]	CIMR RGB Detailed Processing Model	CIMR-COM-ST-RGB-006
[RD32]	CIMR RGB Software Installation and User Manual	CIMR-UM-ST-RGB-009
[RD33]	Map Projections: A Working Manual.	Snyder, J. P. (1987). U.S. Geological Survey Professional Paper 1395. Washington, DC: US Government Printing Office.
[RD34]	A guide to EASE Grids	National Snow and Ice Data Center. (n.d.). *Guide to EASE grids*. Retrieved January 15, 2025, from

		https://nsidc.org/data/user-resources/help-center/guide-ease-grids
[RD35]	National Snow and Ice Data Center. (n.d.). *Guide to NSIDC's polar stereographic projection*.	Retrieved January 15, 2025, from https://nsidc.org/data/user-resources/help-center/guide-nsidcs-polar-stereographic-projection
[RD36]	EASE-Grid 2.0: Incremental but Significant Improvements for Earth-Gridded Data Sets.	Petrov, A., Ai, T., Doytsher, Y., Filin, S., Gómez, C., Koshkariov, A., ... & Weibel, R. (2012). Geospatial semantics. *ISPRS International Journal of Geo-Information, 1*(1), 32–35. https://doi.org/10.3390/ijgi1010032
[RD37]	National Snow and Ice Data Center. (n.d.). *EASE-Grid conversion tools (easegrids-easeconv)*	[GitHub repository]. Retrieved January 15, 2025, from https://github.com/nsidc/easegrids-easeconv
[RD38]	OSGeo. (n.d.). *Stereographic projection source code (stere.cpp)*	[GitHub repository]. Retrieved January 15, 2025, from https://github.com/OSGeo/PROJ/blob/master/src/projections/stere.cpp
[RD39]	OSGeo. (n.d.). *Mercator projection source code (merc.cpp)*	[GitHub repository]. Retrieved January 15, 2025, from https://github.com/OSGeo/PROJ/blob/master/src/projections/merc.cpp
[RD40]	PROJ contributors. (n.d.). *PROJ: Cartographic projections and coordinate transformations library*.	Retrieved January 15, 2025, from https://proj.org/en/stable/

3. Output Grids and Map Projections

The RGB offers a variety of output grids and map projections for L1C interpolations. An overview of grids and projections available to the user are provided in CIMR RGB Software Installation and User Manual [RD29], Tables 2 and 3 respectively. This Section describes the implementation of these grids within the processing pipeline.

The `grid_generation` module contains the definition of the available output grids and projections as well as functionality to create grids and convert coordinates between different projections.

3.1. Generating grids

An example of a grid definition string is provided below for an EASE2 Global 9km grid (`EASE2_G9km`):

```
'EASE2_G9km': {'epsg': 6933,
               'x_min': -17367530.44, 'y_max': 7314540.83,'res': 9008.05,
               'n_cols': 3856, 'n_rows': 1624,
               'lat_min': -86, 'lat_max': 86
              }
```

Upon initiation of the RGB, the user selected grid is queried and samples from the L1b data are removed if they fall out of the boundaries of the grid (See Figure 3).

It is necessary for a grid to be generated in order to interpolate the L1b brightness temperatures onto. The grids are generated in a cartesian coordinate system defined by the input projection (`epsg`), where the upper left corner is equal to the grid (`x_min`, `y_max`). The target locations for the interpolation are defined by the centre of the grid cells, therefore half the grid resolution is added/subtracted from (`x_min`, `y_max`). Following from that definition of (`x_min`, `y_max`), the coordinates of the center of each grid cell is defined as:

$$\begin{aligned} xs[i_{\text{col}}] &= x_{\min} + (i_{\text{col}} * \text{res}) \\ ys[i_{\text{row}}] &= y_{\max} - (i_{\text{row}} * \text{res}) \end{aligned} \tag{3.1}$$

For

$$i_{\text{col}} = 0, \ldots, n_{\text{cols}} - 1, i_{\text{row}} = 0, \ldots, n_{\text{rows}} - 1 \tag{3.2}$$

The procedure outlined above is used for all EASE grids and stereographic grids, for which commonly used grids have already been defined by NASA ([RD34] and [RD35]). For the Mercator grids, in lieu of a standard grid used by the community, it was necessary to create a custom definition. This was achieved by selecting the lon, lat bounds for which the grid was desired, converting to the chosen Mercator projection (See Section 3.2) and then creating the correct number of rows and columns that fit the desired resolution.

Once the grid coordinates have been created, these are considered the “target locations” and are passed through the pipeline. Upon completion of the interpolation, a `cell_row` and `cell_col` variable is provided with the output data, which allows the user to add the interpolated data back onto the chosen grid.

3.2. Converting coordinates between projections

The `grid_generator` module provides functionality to convert between (lon, lat), (x, y) and (row, col) for all provided projections. The `grid_generator` module is frequently called throughout the RGB to convert between these reference frames when it is required or more convenient for a certain numerical operation.

Each of the six projections for which functionality is provided come with its own set of conversion formulas. For the projections used in the EASE grids (Cylindrical Equal Area (CEA), Lambert's Azimuthal Equal Area (LAEA), the conversion formulas were implemented directly according to the formulas outlined in the widely used EASE2 definition paper [RD36]. Moreover, [RD37] was also used as reference.

Upon implementation of the EASE formulas, the use of the PROJ [RD40] package was explored for coordinate conversions. After validation of the CEA and LAEA formulas, it was decided to use the PROJ package for the remaining projections, given its optimisation and wide use within the community.

Therefore, the conversion formulae for Stereographic (`stere`) and Mercator (`merc`) are provided in the PROJ documentation [RD38] and [RD39] respectively.

For a comprehensive overview of projections and their associated transformations, [RD33] serves as an invaluable resource.

4. Regridding Algorithms

The RGB provides functionality for a variety of regridding methods, whose theoretical basis are described in this Section.

All algorithms, except for nearest neighbours, rely on a specific number of input samples (or nearest neighbours) to perform interpolation. The selection of these input samples is determined by two configuration parameters: `search_radius` and `max_neighbours`.

- `search_radius` specifies the area within which the algorithm searches for neighboring samples.

- `max_neighbours` defines the maximum number of neighbours that shall be used for interpolation.

If the number of neighbours found within the specified search radius exceeds the value of `max_neighbours`, the algorithm will select only the closest `N = max_neighbours` samples for interpolation.

4.1. Nearest Neighbour

4.1.1. Statement of Function

The *Nearest Neighbour* (NN) regridding algorithm assigns each point in the target grid the value of the closest point in the source grid. This method is especially useful when precise, discrete values need to be preserved, as it does not involve interpolation or averaging.

4.1.2. Heritage

NN doesn't traditionally have a heritage in formal satellite products due to its simplicity and non-smoothing characteristics. It is, however, the fastest algorithm and is useful for sanity checks in the development of more complex algorithms.

4.1.3. Limitations and Assumptions

This approach is fast and simple but will likely introduce abrupt changes and artefacts in the output data due to the lack of smoothing. Moreover, there will be no reduction in noise by averaging. It also “throws away” the vast majority of available input data, leading to potentially inaccurate output results. However, the effective antenna pattern is only broadened to the size of the output grid cell, as opposed to other methods whose effective pattern is largely widened by considering points far away from the target location.

4.1.4. Approximations

No approximations were made.

4.1.5. Algorithm Definition

The Nearest Neighbour algorithm assigns each point in the target grid the value of the closest point in the source grid. If there are N source samples $\{T_{B1}, \ldots, T_{BN}\}$ that fall within a search radius of a given cell, the corresponding gridded T_B is expressed as

$$T_{Bg} = T_{Bj} \tag{4.1}$$

where T_{Bj} represents the single sample that is radially closest to the grid cell centre.

4.1.6. References

This section is intentionally left blank.

4.2. Drop-in-the-Bucket

4.2.1. Statement of Function

The *Drop-In-the-Bucket* (DIB) algorithm aggregates data from the source grid into the cells of the target grid, effectively “dropping” data points into the nearest target cell without weighting.

4.2.2. Heritage

This algorithm doesn’t have a significant heritage in comparable products but is frequently used in literature as a baseline to compare more complex algorithms.

4.2.3. Limitations and Assumptions

While the effective noise fluctuations in the source measurements are reduced in the averaging process, the effective antenna pattern can be significantly broadened due to equal weights given to source samples that may lie near the cell boundaries, resulting in the gridded result containing radiances from outside the target cell/ search area.

4.2.4. Approximations

No approximations were made.

4.2.5. Algorithm Definition

If there are N source samples $\{T_{B1}, \ldots, T_{BN}\}$ that fall within a target cell/search radius, the corresponding gridded T_B is expressed as

$$T_{Bg} = \frac{1}{N} \sum_{i=1}^{N} \alpha_i T_{Bi} \tag{4.2}$$

where all α_i are equal to 1.

Suppose there are more neighbours in the search radius than the specified N = max_neighbours. Then, the algorithm will consider the closest N neighbours.

4.2.6. References

This Section is intentionally left blank.

4.3. Inverse Distance Squared

4.3.1. Statement of Function

The *Inverse Distance Squared* (IDS) regridding algorithm interpolates values from the source grid to the target grid by weighting each source point's influence on the target cell inversely to the square of the distance. Closer points have a much stronger influence than those far away, resulting in smooth gradients across the grid.

4.3.2. Heritage

This algorithm is often used in microwave radiometry applications, most notably in the SMAP L1C Radiometer Half-Orbit 36 km EASE-Grid Brightness Temperatures (BTs) [RD14] product.

4.3.3. Limitations and Assumptions

IDS can introduce smoothing that can mask finer details in the data, especially in the case where source data is unevenly distributed, as is of course the case for conically scanning radiometers. This algorithm is limited in cases where finer resolution detail is required and/or when an appropriate number of neighbouring samples are not within an appropriate proximity to the target cell. This is due to the fact that the sample temperatures are treated as discrete temperatures at that location, as opposed to methods utilising antenna patterns, which allow the distribution of temperatures over larger regions.

4.3.4. Approximations

No approximations were made.

4.3.5. Algorithm Definition

The Inverse Distance Squared method assigns weights to each measurement identified in the points selection depending on its vicinity to the centre of the target output cell.

$$T_{B_{target}} = \frac{1}{A}\sum_{i=1}^{N}\alpha_i T_{Bi_{source}} \tag{4.3}$$

$$A = \sum_{i=1}^{N}\alpha_i \tag{4.4}$$

$$\alpha_i = \frac{1}{d_i^2} \tag{4.5}$$

where d is the orthodromic distance based on the Earth's sphere.

4.3.6. References

The reader is referred to [RD14] and [RD15] for further information.

4.4. Backus Gilbert

4.4.1. Statement of Function

The *Backus-Gilbert* (BG) regridding algorithm interpolates values from the source grid to the target grid by constructing a weighted average of the source points, with weights designed to minimise the fit error and computed taking into account the projection of the source and target antenna gain on the Earth surface. The technique aims to provide an output that would be as close as possible to what would have been measured had the radiometer actually made the measurements with the interpolation point as its boresight centre. The algorithm utilises the non-uniform nature of conical microwave radiometer measurements, where there is oversampling in space.

4.4.2. Heritage

The Backus-Gilbert interpolation algorithm was first developed in the 1960s in order to better understand the internal structure of the Earth. Since its first development, the BG method has been widely used in a variety of scientific fields, mostly in geophysics and, more recently, in the field of spatial data interpolation and resolution enhancement. The algorithm was selected for implementation in the RGB as a result of a literature review of state-of-the-art algorithms, detailed in the *Comparative Performance Assessment Plan* [RD29].

In the last 15 years or so, BG has been extensively researched in the application of microwave radiometry and applied as the chosen interpolation method for a variety of satellite data products.

Most notably, the BG algorithm was used in the creation of the "GCOM-W1 AMSR2 Level 1R Product" and the "SMAP Enhanced L1C Radiometer Half-Orbit 9 km EASE-Grid Brightness Temperatures" and has also been applied to the *Microwave Imager* (MWI) and *Ice Cloud Imager* (ICI) L2 products [RD6].

4.4.3. Limitations and Assumptions

Despite its powerful capabilities, the Backus-Gilbert method has faced challenges in widespread adoption, primarily due to its computational cost and complexity in implementation, especially for large-scale problems.

Implementations of the Backus-Gilbert method in satellite data processing have had to address issues such as artefact production due to poor condition numbers in matrix inversions. This is especially true when the number of neighbours taken into account for the interpolation is large, making the matrix inversion more computationally intensive and affected by uncertainties.

As multiple input source samples are used for the interpolation, the temperatures are averaged temporally over these source samples. It is, therefore, assumed that the surface characteristics remain constant over this period. This assumption is, of course, more applicable in the case where adjacent samples from the same scan are considered. However, there could be significantly more time in-between two samples in which one was taken from a forward-looking part of one scan and the backward-looking part of another. The user should consider this in their choice of configuration parameters.

4.4.4. Approximations

Several approximations are required in order to implement the BG algorithm for the interpolation of radiometric data, in particular when there is a large number of high-resolution measurements, entailing a higher computational load.

Antenna patterns for CIMR are provided with high resolution (< 0.01 deg for K and Ka bands) through the full forward hemisphere. Projecting all the gain values on Earth's surface for each source pattern is not feasible, and the following strategies are adopted to decrease the computational load:

- Antenna patterns are sub-sampled to lower resolution
- Values gain smaller than a threshold values are set to zero
- Antenna patterns are projected to an integration grid on the Earth's surface (with resolution being a user-defined parameter), which could downgrade further the antenna pattern resolution

Antenna temperature measurements, described by 4 Stokes parameters, are, in principle, obtained via a radiative transfer calculation, which can be described with a Mueller Matrix. The full Mueller matrix for the SMAP and CIMR instrument is provided and can be included in the BG algorithm when

interpolating the 4 Stokes parameters. However, this significantly increases the amount of operations in the projection step since all 16 values of the Mueller matrix need to be projected to Earth and recomputed in a Ludwig-3 polarisation basis relative to the Earth's surface. Therefore, an approximation is performed that derives a scalar value from the Mueller matrix to characterise the antenna gain, as described in Section 5.3. This considerably speeds up the calculation, with the drawback that all 4 Stokes parameters will be interpolated with the same scalar value of the gain, neglecting the different response of the feedhorn to different polarisation components.

4.4.5. Algorithm Definition

The T_B measured by a receiving antenna is expressed as

$$T_B = \iint G(x,y) T_B(x,y)\, dx\, dy = \int G(\rho) T_B(\rho)\, ds \tag{4.6}$$

where $G(x,y) = G(\rho)$ is the projected antenna pattern on Earth, i.e., the gain of the antenna at position $(x,y) = \rho$ on the Earth's Surface, and $T_B(x,y) = T_B(\rho)$ is the microwave energy emitted from the point ρ. $G(\rho)$ is the normalised gain value of the antenna, where $\int G(\rho) dS = 1$.

For the interpolation of an output grid cell, multiple source samples and their respective antenna patterns are considered, each with varying positions and rotations on the 2D surface. The set of source patterns considered is expressed as:

$$T_{B_{\text{source},i}} = \int G_{\text{source},i}(\rho) T_{B_{\text{source},i}}(\rho)\, dS \tag{4.7}$$

where $G_i = (i = 1,\ldots, N)$.

The target measurement, $T_{B_{target}}$, is measured by another receiving antenna pattern. Depending on the desired output grid type, this could be the real or simulated antenna pattern of the target band in the case of an L1R remap or a gaussian fit to the size of the output cell in the case of an L1C remap. The target measurement is expressed as

$$T_{B_{\text{target}}} = \int F_{target}(\rho) T_{B_{\text{target}}}(\rho)\, dS \tag{4.8}$$

where $F(\rho)$ is the target antenna pattern and $\int F(\rho) dS = 1$.

$T_{B_{target}}$ is a weighted combination of the source samples expressed as

$$T_{B_{target}} = \sum_{i=1}^{N} a_i T_{B_{source,i}} = \sum_{i=1}^{N} a_i \left(\int_S G_i(\rho) T_{B_{source,i}}(\rho) dS \right) \tag{4.9}$$

where a_i are weighting factors of the source samples, that can be computed to minimise the fit error.

The ideal a_i should satisfy a fit error of zero,

$$F(\rho) - \sum_{i=1}^{N} a_i G_i(\rho) = 0 \tag{4.10}$$

The resulting equation for the weighting factors (written in matrix form) is

$$\mathbf{a} = \mathbf{V}^{-1} \left[\mathbf{v} + \left(\frac{1 - \mathbf{u}^T \mathbf{V}^{-1} \mathbf{v}}{\mathbf{u}^T \mathbf{V}^{-1} \mathbf{u}} \right) \mathbf{u} \right] \tag{4.11}$$

where

$$\mathbf{V} = \mathbf{G} + k\mathbf{I} \tag{4.12}$$

$$u_i = \int G_i(\rho) dS \tag{4.13}$$

$$v_i = \int G_i(\rho) F(\rho) dS \tag{4.14}$$

$$G_{ij} = \int G_i(\rho) G_j(\rho) dS \tag{4.15}$$

k is a factor multiplied by the identity matrix I, which varies from 0 to infinity and smooths the variation of the coefficient a_i.

4.4.6. References

For further reading on the BG algorithm, we refer the reader to [RD1], [RD2], [RD3], [RD4], [RD5], [RD6], [RD7], [RD10], [RD16] and [RD17].

4.5. Radiometer Scatterometer Image Reconstruction

4.5.1. Statement of Function

The *radiometer Scatterometer Image Reconstruction* (rSIR) method is an iterative image reconstruction technique. rSIR makes use of a surface temperature distribution defined by the instruments' antenna patterns. The algorithm uses regularisation in order to trade-off between noise amplification and spatial resolution. It achieves this by selecting an appropriate number of iterations, which consequently produces only a partial reconstruction of the image.

The aim is to estimate the surface brightness temperature based on the noisy source measurements. The algorithm makes use of the instruments (or simulated) antenna patterns, which translate to the *Measurement Response Function* (MRF) on the Earth's surface and is therefore highly sensitive to processing decisions pertaining to this. The MRF is calculated using the satellite position, antenna scan angle, and the antenna gain pattern. The processing of antenna patterns and their associated MRF's is discussed in Section 5.5.

4.5.2. Heritage

rSIR was selected as an outcome of a literature study on state-of-the-art regridding algorithms outlined in the *Comparative Performance Assessment Plan* [RD29]. The studies by Long et al. [RD21, RD22] applied to SMAP data demonstrate that in comparison with other image production methods, rSIR produces images with finer resolution and lower *Root Mean Square Errors* (RMSEs). rSIR, in particular, exhibits slightly lower noise in simulations and finer resolution by certain metrics. The studies conclude that due to its lower computational requirements and superior performance, rSIR is preferred for generating enhanced-resolution images for Calibrated Passive Microwave Daily Equal-Area Scalable Earth Grid 2.0 (EASE2) Brightness Temperature (CETB) products, specifically for SMAP applications.

rSIR has been applied to SMAP data in a stand-alone NSIDC product, "SMAP Radiometer Twice-Daily rSIR-Enhanced EASE-Grid 2.0 Brightness Temperatures" [RD19]. This product (and its associated documentation) was one of the main sources of reference in the implementation of this algorithm.

4.5.3. Limitations and Assumptions

As the rSIR algorithm is an iterative update of temperature distribution over a larger area surrounding the target location, it is only appropriate to apply it to the brightness temperatures (`bt_h`, `bt_v`, `bt_3`, `bt_4`). Therefore, all other variables apart from these use IDS for their regrid when this algorithm is selected.

As multiple input source samples are used to reconstruct the image, the reconstructed image averaged temporally over these source samples. It is, therefore, assumed that the surface characteristics remain constant over this period. This assumption is, of course, more applicable in the

case where adjacent samples from the same scan are considered. However, there could be significantly more time in-between two samples in which one was taken from a forward-looking part of one scan and the backward-looking part of another. The user should consider this in their choice of configuration parameters.

4.5.4. Approximations

If a full reconstruction was employed, noise in the source samples could be excessively amplified; the algorithm is therefore regularised by the use of the iteration number, which effectively imposes a smoothing constraint on the image.

The antenna pattern processing and, consequently, MRF contains a degree of approximation, regardless of the method chosen to generate them (users can use instrument antenna patterns or simulate a Gaussian; see the *Software Installation and User Manual* [RD32] for more details). In all cases, users need to choose a gain threshold (which ignores the antenna pattern below a certain gain value) to be considered as a "footprint". This is generally considered in the field to be 3dB (or half power). Moreover, in the case that "instrument" antenna patterns are used, some interpolation is applied to the patterns before ingestion into the RGB, and in the case "gaussian" or "gaussian_projected" patterns are selected, the antenna pattern itself is of course approximated with a gaussian function (see Sections 5.5.1 to 5.5.3 for detail on this function). The MRF is further approximated in its superposition to the image domain/integration grid. The resolution of this grid is user-configurable.

4.5.5. Algorithm Definition

The target surface brightness temperature distribution $T_{B,\,target}(x,\,y)$ is treated as a discrete signal, sampled at the chosen grid pixel spacing, and is estimated from N source measurements $T_{B,\,source}$. $T_{B,\,target}(x,\,y)$ is considered over an image domain, N_x x N_y, large enough to contain all considered samples and associated antenna patterns for the interpolation of a target output cell. $T_{B,\,target}(x,y)$ is vectorised over this domain, $a_j = T_{B,\,target}(x_j, y_j)$, where $j = l + N_x k$ and $l,\ k$ correspond to the row and column number of the pixel in the image domain. The image domain is analogous to what is otherwise referred to in this report as the 'integration grid'. The creation of this is described in Section 5.4.

A particular measurement, z_i, can be expressed as

$$z_i = \sum_{j \in \text{image}} h_{ij} a_j \tag{4.16}$$

where $h_{ij} = MRF(x_l, y_k)$, or the normalised antenna pattern projected to Earth evaluated at the j^{th} pixel centre. The MRF is negligible at a certain distance from the pixel centre and is cut to a

user-selected value, and the sum is therefore only computed over an area local to the measurement position. The h_{ij} are normalised such that $\sum_j h_{ij} = 1$.

For all measurements considered for a target output cell,

$$\vec{T} = \mathbf{H}\vec{a} \tag{4.17}$$

where H contains the samples MRF for each measurement, and T and a are vectors composed of the measurements z_i, and the samples surface brightness temperatures a_j, respectively.

The rSIR algorithm solves this equation iteratively. It approximates a maximum-entropy solution to an underdetermined system and a least-squares solution to an overdetermined system.

The first iteration is a simple estimate of $T_{B,target}$ with the j^{th} pixel, expressed as:

$$a_j^0 = \frac{\sum_i h_{ij} z_i}{\sum_i h_{ij}} \tag{4.18}$$

At the kth ($k > 0$) iteration, the forward projection and scale factor are defined as:

$$f_i^k = \frac{\sum_n h_{in} a_n^k}{\sum_n h_{in}} \tag{4.19}$$

$$d_i^k = \sqrt{\frac{z_i}{f_i^k}} \tag{4.20}$$

respectively, where n is the index to each pixel in the image. The non-linear update term is expressed as:

$$u_{ij}^k = \begin{cases} \left[\frac{1}{2} f_i^k \left(1 - \frac{1}{d_i^k}\right) + \frac{1}{a_j^k d_i^k}\right]^{-1}, & \text{if } d_i^k \geq 1 \\ \left[\frac{1}{2} f_i^k \left(1 - d_i^k\right) + a_j^k d_i^k\right], & \text{if } d_i^k < 1 \end{cases} \tag{4.21}$$

and the jth image pixel is computed as:

$$a_j^{k+1} = \frac{\sum_i h_{ij} u_{ij}^k}{\sum_i h_{ij}} \tag{4.22}$$

This set of equations is iterated over k for the user-selected N iterations. The set of equations is minimised by cutting the MRF to within a certain user-selected value of the peak response and set to

zero elsewhere. The set of input samples and associated MRFs input to the algorithm are calculated based on the satellite position and scan angle and will have different characteristics (ellipticity, rotation, footprint size) depending on satellite position, the band (antenna pattern) in question, and gain threshold considered.

The final output temperature is calculated by combining the target MRF and iterated temperature distribution:

$$T_{B_{target}} = \sum_{j \ \epsilon \ image} h_{j_{target}} a_j^{k+1} \tag{4.23}$$

4.5.6. References

For further reading on the rSIR algorithm, the reader is referred to [RD4], [RD18], and [RD19].

4.6. Landweber and Conjugate Gradients

4.6.1. Statement of Function

Landweber (LW) and *Conjugate Gradients* (CG) are iterative methods, i.e., image reconstruction algorithms that iteratively refine an estimated solution by minimising the difference between the measured data and the forward projection of the estimated image. The algorithm applies a gradient descent approach to adjust the estimate at each iteration, optionally incorporating regularisation techniques (such as Tikhonov regularisation) to suppress noise and enhance stability.

4.6.2. Heritage

The Landweber method was selected following a review of iterative image reconstruction techniques suitable for solving ill-posed inverse problems [RD29] - *Comparative Performance Assessment Plan*. Originally proposed by Landweber (1951), this gradient-descent-based approach has been widely utilised in fields such as medical imaging, astronomy, and geophysics due to its simplicity and flexibility. The original LW approach has a relatively slow convergence rate that hampers its utility in real-world scenarios, and improved versions, such as the one proposed by Lenti et al. [RD20] for simulated radiometric data, feature regularisation terms that improve the stability of the solution and number of iterations to convergence.

The Conjugate Gradients iterative method is a valid alternative for matrix inversion problems, originally developed for solving systems of linear equations. In particular, the *Conjugate Gradients Normal Equations* (CGNE) variant, which is tailored for least-squares problems, has been widely applied in areas such as geophysical inversion, tomography, and image deblurring.

4.6.3. Limitations and Assumptions

The computational complexity of iterative inversion methods scales with the size of the input data. In the case of radiometer data, each measurement is a result of the convolution with the antenna pattern gain, which can cover a large area of Earth's surface. Hence, the resulting matrix to be inverted can have thousands of rows and columns, which makes the calculation extremely challenging. In addition, a large number of iterations is typically required to reach convergence, posing limitations on the accuracy that can be achieved. Finally, the fact that the problem is inherently ill-posed implies that a unique and stable solution is not granted. Regularisation ameliorates this issue, but a fine-tuning of the algorithm parameters is required (such as step size and regularisation parameter).

4.6.4. Approximations

The projection of antenna patterns on the Earth's surface is required for this algorithm, so the same approximations as in Section 4.4.4 are applied.

4.6.5. Algorithm Definition

The T_B measured by a receiving antenna is expressed as

$$T_B = \iint G(x,y) T_B(x,y)\, dx\, dy = \int G(\rho) T_B(\rho)\, ds \tag{4.24}$$

where $G(x,y) = G(\rho)$ is the projected antenna pattern on the Earth's surface. The problem can be discretized by assuming a grid on the Earth's surface. If each pixel of the grid is determined by the indexes (i,j), then for each measurement k:

$$T_{B,k}^{\text{measure}} = \sum_{ij} G_{ij}^{k} T_{B,ij}^{\text{image}} \tag{4.25}$$

And by re-ordering the arrays on the right-hand side:

$$T_{B,k}^{\text{measure}} = \sum_{i} G_{i}^{k} T_{B,i}^{\text{image}} \tag{4.26}$$

Which can be written in matrix form as

$$T_{B}^{\text{measure}} = G T_{B}^{\text{image}} \tag{4.27}$$

In this way, the original regridding problem becomes a matrix inversion problem.

4.6.5.1. Landweber

The LW algorithm looks for an approximate solution of the system of linear equations represented by the equation $Y = AX$. This is done iteratively by choosing an initial guess X_0 (usually an array of zeros) and then computing the update to the solution with:

$$X_{k+1} = X_k - \omega A^*(AX_k - Y) \tag{4.28}$$

Where A^* is the adjoint matrix (complex conjugate and transpose) and ω is the step size, usually chosen in the range $0 < \omega < 1/||A^*A||^2$. If a regularisation term is added, the iteration step becomes:

$$X_{k+1} = X_k - \omega \left(A^*(AX_k - Y) + \lambda X_k\right). \tag{4.29}$$

4.6.5.2. Conjugate Gradients Method

Consider first a squared matrix *A*. The initial residual is

$$r_0 = Y - AX_0 \tag{4.30}$$

The initial update direction is $p_0 = r_0$ and the initial guess X_0 is usually an array of zeros. These variables (residual, update direction, and solution) are then updated in the following way:

$$\alpha_k = \frac{r_k^T r_k}{p_k^T A p_k} \tag{4.31}$$

$$X_{k+1} = X_k + \alpha_k p_k \tag{4.32}$$

$$r_{k+1} = r_k - \alpha_k A p_k \tag{4.33}$$

$$p_{k+1} = r_{k+1} + \frac{r_{k+1}^T r_{k+1}}{r_k^T r_k} p_k \tag{4.34}$$

In the most general case of a non-squared matrix, multiplying both members of the equation $Y = AX$ by A^T, we obtain $A^TY = A^TAX$ where the matrix A^TA is squared. So, the algorithm can be applied in the same way by substituting A with A^TA.

Finally, a regularisation term can be included when computing residual:

$$r_k = Y - AX_k - \lambda X_k \tag{4.35}$$

References

For further reading on this algorithm, the reader is referred to [RD5], [RD20], [RD23], [RD24].

4.7. NEDT and Uncertainty Propagation

The uncertainties output as a result of the regridding algorithms is provided in this Section. The uncertainty calculations are limited to that added as a result of the regridding algorithm only. An additional source of uncertainty in the regridded L1r/c measurement results from the uncertainty of the antenna pattern gains, the interpolation of the antenna patterns to a coarser resolution, and the projection of the antenna pattern to Earth.

As the antenna patterns utilised come without documentation/ description of uncertainty, and the L1b data for all instruments is provided without uncertainty quantifications for the position, velocity, or attitude of the satellite, it has been decided not to include these considerations in the approximation.

A covariance matrix is required for uncertainty propagation for some of the regridding algorithms. The L1b NEDT and the uncertainty correlation of neighbouring arc samples are the focus of an ongoing *Metrological Analysis of CIMR RADiometry* (MACRAD) study. This study will provide look-up tables translating an L1b BT to NEDT, as well as the uncertainty correlations between the same scan samples. In the absence of deliverables from this study, the per band NEDT cited in the [RD26] is applied along the diagonals of the covariance matrix.

In the meantime, a configuration parameter is available <antenna_pattern_uncertainty>, which is defined as a single value corresponding to the total uncertainty considered as a result of the antenna pattern and associated processing. When a value is used for this configuration parameter its value is added to the NEDTs calculated below according to the Equation 4.36.

$$NEDT_{out} = \sqrt{NEDT_{BT}^2 + NEDT_{AP}^2} \tag{4.36}$$

4.7.1. Nearest Neighbour

As only a single sample is used in the regrid, the resulting value retains the same noise as the input sample, which is expressed as:

$$\sigma_{\text{eff}}^2 = \sigma^2 \tag{4.37}$$

4.7.2. Drop-in-the-Bucket

The uncertainty of the gridded T_B is expressed as:

$$\sigma_{T_{Bg}}^2 = \frac{1}{N^2} \sum_{i=1}^{N} \sigma_{T_{Bi}}^2 \tag{4.38}$$

4.7.3. Inverse Distance Squared

The uncertainty of the output measurement is expressed as:

$$\sigma_{T_{B_{target}}} = \frac{1}{A}\sqrt{\sum_{i=1}^{N} \alpha_i^2 \sigma_{T_{Bi_{source}}}^2} \tag{4.39}$$

4.7.4. Backus Gilbert

The resulting uncertainty of the output measurement is

$$\sigma_T^2 = \mathbf{a}^T \mathbf{E} \mathbf{a} \tag{4.40}$$

where **E** is the measurement error covariance matrix, and **a** is the vector of weights as defined in Sec. 4.4.5. A look-up table of measurement errors will be provided at some point via the MACRAD project; in the meantime, the NEDT stated for each band in the [RD26] will be used along the diagonals of **E**.

4.7.5. Radiometer Scatterometer Image Reconstruction

Propagating the uncertainty through this algorithm is not trivial. This is due to the non-linear update term, u_{ij}^k. Mathematical formulations for the propagation were considered; however, this poses challenges in uncertainty as non-linear functions can distort input distributions, have variable sensitivity across their domain, and introduce complex interactions between variables. Moreover, a method could not be found in the literature considered for this report. In addition, there is no mention of uncertainty in the rSIR SMAP product [RD18, RD19], and indeed uncertainty variables are not provided in its output.

It was decided at this stage to propagate uncertainty for rSIR following the same propagation formulas as IDS (see Section 4.7.3). The proportion of the antenna pattern considered for the output temperature is dependent on its proximity to the output location and it is therefore considered reasonable to propagate the uncertainty in this way.

4.7.6. Landweber

Landweber algorithm is a linear iterative method, so uncertainty can be propagated through each iteration in the following manner:

$$E_X^{(k+1)} = \omega^2 A^* E_Y A + [I - \omega(A^*A + \lambda I)] E_X^{(k)} [I - \omega(A^*A + \lambda I)]^* \tag{4.41}$$

Where E_Y is the covariance matrix associated with the input data, I is the identity matrix, ω, λ and A are as defined in Sec. 4.6.5.1. The equation above can be derived directly from the iterative step by applying the rule for propagation of the covariance matrix:

$$Y = AX \longrightarrow E_Y = AXA^T \tag{4.42}$$

Finally, the gridded output uncertainty is obtained from the diagonals of E, which represent the calculated uncertainty for each output grid cell.

4.7.7. Conjugate Gradients

The iterative step in the CG algorithm is more complex than LW, so an accurate propagation of the covariance matrix is mathematically elaborated and computationally heavy. The following simplification is adopted by assuming that the uncertainty on the parameter α_k is negligible:

$$E(r_0) = E(Y) \tag{4.43}$$
$$E(p_0) = A^T E(r_0) A \tag{4.44}$$
$$E(X_{k+1}) = E(X_k) + \alpha_k E(p_k) \tag{4.45}$$
$$E(r_{k+1}) = E(r_k) - \alpha_k A E(p_k) A^T \tag{4.46}$$
$$E(p_{k+1}) = A^T E(r_{k+1}) A \tag{4.47}$$

where all parameters are as defined in Sec. 4.6.5.2. The gridded output uncertainty is obtained from the diagonals of E, which represent the calculated uncertainty for each output grid cell.

5. Implementation

5.1. Algorithm Flow

The toolbox is governed and initiated with the use of a configuration file, which provides users with a variety of options. Figure 1 depicts the flow of data through the toolbox. The white boxes indicate functions that sit within the coloured processing modules. The toolbox has been designed such that input data types, ingestion functionality, regridding algorithms, and modular functionality, in general, can be added relatively easily. It is also intended that the modules can be used independently or outside of the main pipeline.

As can be seen from Figure 1, there are no corrections implemented on the data, such as land/water contamination, atmospheric, faraday rotation etc.

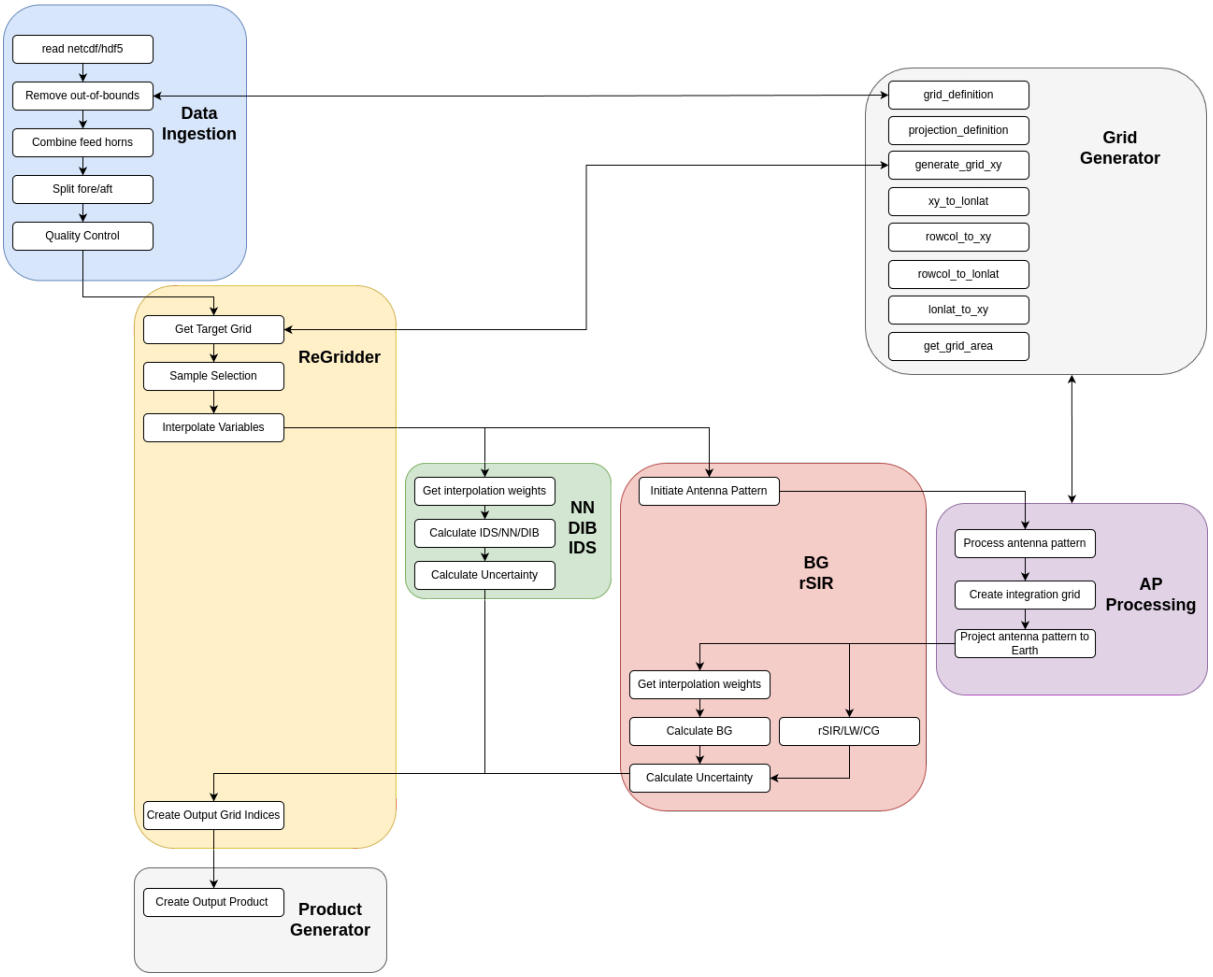

Figure 1 - Diagram of the data flow in the toolbox

5.2. Points Selection

The points selection algorithm lies within the `ReGridder` module and utilises the `pyresample python` library. The search radius and the number of neighbours desired are user-configurable. `pyresample` calculates orthodromic distances of the Earth's surface based on spherical geometry. At the time of writing, the points selected for use in the regridding algorithm are based solely on the proximity to the target location, as opposed to considering scan numbers or feed horn numbers when selecting points.

5.3. Initializing Antenna Patterns

Antenna patterns need to be initialised before being projected to the Earth's surface.

1. The functional shape of the antenna pattern in spherical coordinates is decided based on the chosen projection method (see Section 5.5)
2. All values of the gain for $\theta > \theta_{max}$ are set to zero (where the parameter θ_{max} is configurable by the user, and a value of 40° is recommended, as usually, no feedhorn has a significant value of the gain at such an angle)
3. All values of the gain smaller than a user-defined threshold are set to zero
4. The value of the power above the threshold is saved so that it can be used to scale the projected antenna pattern later in the pipeline.
5. An antenna pattern radius is defined by estimating the largest radius on Earth where the gain is non-zero (i.e., above the threshold), as shown in the figure below.

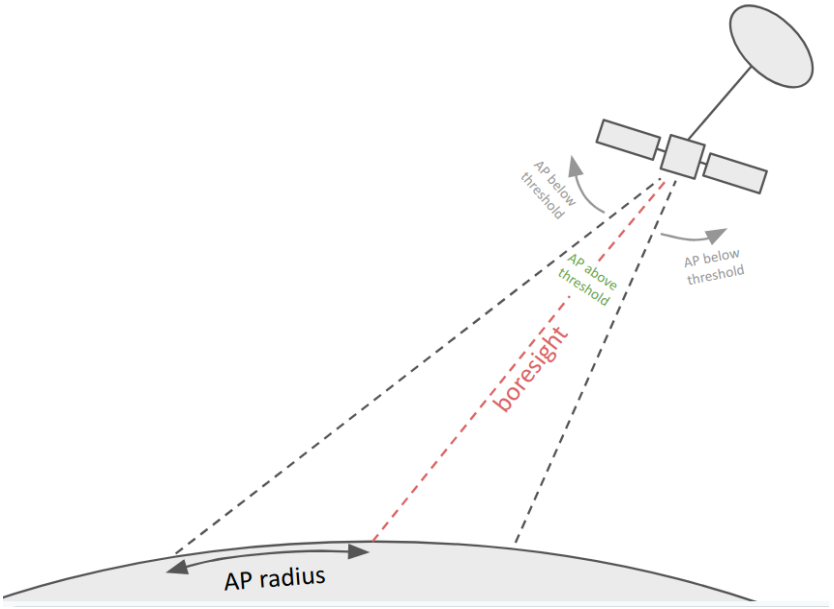

Figure 2 - Sketch of the procedure to estimate the AP (antenna pattern) radius. First, the boresight of the antenna feedhorn is intersected with the Earth's surface. Then, the distance on Earth with the

furthest point with above-threshold projected gain is measured. For this approximate calculation, the Earth is assumed to be a sphere.

Antenna patterns are fully characterised by four values of the gain: H-pol cross-pol, H-pol co-pol, V-pol cross-pol, V-pol co-pol. These four values allow the definition of a 4 x 4 Mueller matrix, which is required to compute the response of the optical system to the incoming polarised radiation. Due to the additional computational cost of projecting the full Mueller matrix to Earth, we derive a scalar value of the gain by averaging the cross and co-polarisation terms. The full Mueller matrix is expressed as:

$$\mathbf{G} = \begin{bmatrix} |G_{vv}|^2 & |G_{vh}|^2 & \mathrm{Re}(G_{vv}G_{vh}^*) & \mathrm{Im}(G_{vh}G_{vv}^*) \\ |G_{vh}|^2 & |G_{hh}|^2 & \mathrm{Re}(G_{hh}G_{vh}^*) & \mathrm{Im}(G_{hh}G_{vh}^*) \\ 2\mathrm{Re}(G_{vv}G_{vh}^*) & 2\mathrm{Re}(G_{vh}G_{hh}^*) & \mathrm{Re}(G_{vv}G_{hh}^* + G_{vh}G_{vh}^*) & -\mathrm{Im}(G_{vv}G_{hh}^* - G_{vh}G_{vh}^*) \\ 2\mathrm{Im}(G_{vv}G_{vh}^*) & 2\mathrm{Im}(G_{vh}G_{hh}^*) & \mathrm{Im}(G_{vv}G_{hh}^* + G_{vh}G_{vh}^*) & \mathrm{Re}(G_{vv}G_{hh}^* - G_{vh}G_{vh}^*) \end{bmatrix} \tag{5.1}$$

where Re and Im represent the real and imaginary components respectively. The total scalar gain measured for incoming H-polarized radiation is $G_{\mathrm{H}} = \sqrt{G_{hh} + G_{hv}}$ and similarly for the gain measured for incoming V-polarized radiation $G_{\mathrm{V}} = \sqrt{G_{vv} + G_{vh}}$. Thus, the scalar gain can be estimated as an average of H and V modes:

$$G_{\mathrm{scalar}} = \frac{1}{2}\left(\sqrt{G_{hh} + G_{hv}} + \sqrt{G_{vh} + G_{vv}}\right) \tag{5.2}$$

5.4. Image Domain/ Integration Grid

A temporary integration grid is used for calculations involving projected antenna patterns. This is required by the following algorithms:

- BG/rSIR: for each output grid cell (L1c) or output antenna pattern (L1r), the neighbouring antenna patterns are projected to the integration grid so that the integrals in Sec. 4.4.5 can be computed; the size of the integration grid is such that all projected patterns fit in the grid, taking into account their radius (estimated as explained in Sec. 5.3, point 5)

- Iterative inversion methods (LW, CG): the output grid is divided into chunks for memory optimisation, and an integration grid is defined to include any antenna pattern lying entirely or partially in the chunk.

Since the integration grid is needed only for the purpose of performing intermediate calculations, it is not required to be of the same type as the user-selected output grid. For this reason, we chose an EASE2 grid for this purpose, which has a mathematically simple definition and it is convenient for computing integrals being an equal-area projection.

The resolution of the integration grid can be configured by the user. The choice of the resolution depends on the band of the data to be regridded (and the target band as well, for L1b → L1r) since it should be high enough to resolve the projection of the antenna patterns to Earth (Ka-band data will require resolution smaller than 1 km, while L-band data can be regridded with 3km). The following resolutions are recommended for each band and allow to resolve the main lobe of the antenna pattern with more than 30 pixels:

Table 1 - Integration Grid Recommended parameters

Instrument/Band	Integration Grid Resolution
SMAP band L	3 km
CIMR band L	3 km
CIMR band C	1.5 km
CIMR band X	1 km
CIMR band K	0.5 km
CIMR band Ka	0.25 km

5.5. Antenna Pattern Projection and Measurement Response Function

The projection of antenna patterns to Earth, the result of which is known as the Measurement Response Function, can be performed according to 3 user-selected techniques:

- Gaussian
- Gaussian_projected
- Instrument

5.5.1. Gaussian

The “gaussian” projection technique is a simplified version of the antenna pattern projection, intended for situations in which a shorter computational time is desired, as well as allowing developers/users to remove performance sensitivities to antenna patterns and their projections when comparing regridding algorithms. Projection from the antenna to Earth is not performed, and the MRF is built directly on the Earth's surface. The antenna pattern for a measurement at location (x_0, y_0) is assumed to be a 2D gaussian on the integration grid, defined by the equations:

$$G = \exp\left[-(x_1^2/2\sigma_x^2 + y_1^2/2\sigma_y^2)\right] \tag{5.3}$$

$$x_1 = (x - x_0)\cos\alpha + (y - y_0)\sin\alpha \tag{5.4}$$

$$y_1 = -(x - x_0)\sin\alpha + (y - y_0)\cos\alpha \tag{5.5}$$

with the following parameters:

- The standard deviation of the two perpendicular directions (σ_x and σ_y) are defined by the user and should be chosen based on the instrument and band under consideration.

- The rotation angle α with respect to the latitude line passing through (x_0, y_0) is computed to take into account the satellite position and the boresight corresponding to the selected feedhorn.

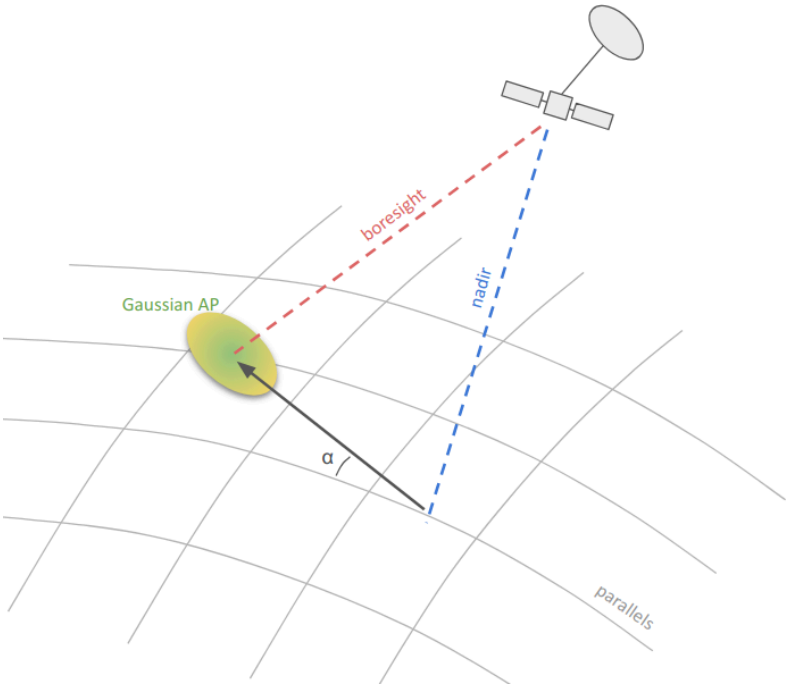

Figure 3 - Sketch showing how the rotation angle α of the 2D gaussian is computed when using the "gaussian" projection method for antenna patterns.

5.5.2. Gaussian_projected and Instrument (CIMR)

These two methods employ the same technique for the projection of the antenna pattern. The only difference is in the assumed functional shape of the antenna pattern in the antenna reference frame. For "gaussian_projected", the antenna pattern is a gaussian in the (θ, ϕ) spherical coordinate system, with user-defined variance (σ_θ and σ_ϕ). For "instrument", the antenna pattern is loaded from the actual beam files of the radiometers (SMAP, CIMR).

Subsequent to either loading the beam file or the creation of a gaussian in its place, the patterns are projected to the Earth's surface. The projection algorithm requires the following values, all obtained from L1b data:

- The position (x_0, y_0, z_0) of the satellite at the moment of the measurement (in an ECEF coordinate system)
- The attitude matrix A of the satellite in an ECEF coordinate system (CIMR, not available for SMAP)
- The scan angle θ_{scan}

and the following specifications of the radiometer:

- The tilt angle θ_{tilt}
- The feedhorn offsets (θ_{off}, ϕ_{off})

A value for the projected antenna pattern needs to be computed for each cell (i,j) of the integration grid. To this extent, the following operations are performed for each (i,j):

1. Convert the coordinates (longitude, latitude) of the point (i,j) to ECEF coordinates (x, y, z)
2. Define the vector $\mathbf{p} = (x_p, y_p, z_p)$ pointing from the satellite position (x_0, y_0, z_0) to (x, y, z) and normalise it to 1.
3. Bring $\mathbf{p}$ into the satellite reference body frame via its attitude matrix:

$$\mathbf{p}' = A\mathbf{p} \tag{5.6}$$

4. Define the antenna reference frame, as the frame with the following axis (coordinates are expressed in the satellite body frame)

$$\mathbf{y}_{\text{antenna}} = [-\cos(\theta_{\text{tilt}} + \theta_{\text{off}})\cos(\theta_{\text{scan}} + \phi_{\text{off}}),\ \cos(\theta_{\text{tilt}} + \theta_{\text{off}})\sin(\theta_{\text{scan}} + \phi_{\text{off}}),\ \sin(\theta_{\text{tilt}} + \theta_{\text{off}})] \tag{4.7}$$

$$\mathbf{z}_{\text{antenna}} = [-\sin(\theta_{\text{tilt}} + \theta_{\text{off}})\cos(\theta_{\text{scan}} + \phi_{\text{off}}),\ \sin(\theta_{\text{tilt}} + \theta_{\text{off}})\sin(\theta_{\text{scan}} + \phi_{\text{off}}),\ -\cos(\theta_{\text{tilt}} + \theta_{\text{off}})] \tag{4.8}$$

$$\mathbf{x}_{\text{antenna}} = \mathbf{y}_{\text{antenna}} \times \mathbf{z}_{\text{antenna}} \tag{4.9}$$

5. Compute the polar angles (θ, ϕ) of $\mathbf{p}'$ in the antenna reference frame:

$$x_{p,\mathrm{ant}} = \mathbf{p}' \cdot \mathbf{x}_{\mathrm{antenna}} \tag{5.10}$$

$$y_{p,\mathrm{ant}} = \mathbf{p}' \cdot \mathbf{y}_{\mathrm{antenna}} \tag{5.11}$$

$$z_{p,\mathrm{ant}} = \mathbf{p}' \cdot \mathbf{z}_{\mathrm{antenna}} \tag{5.12}$$

$$\theta = \arccos\left(z_{p,\mathrm{ant}}\right) \tag{5.13}$$

$$\phi = \mathrm{sgn}(y_{p,\mathrm{ant}})\ \arccos\left(x_{p,\mathrm{ant}} / \sqrt{x_{p,\mathrm{ant}}^2 + y_{p,\mathrm{ant}}^2}\right) \tag{5.14}$$

6. The corresponding value of the antenna gain is inferred by interpolating the antenna pattern data in (θ, ϕ)

7. The value of the gain is re-scaled by multiplying by a factor $\cos\theta_{\mathrm{inc}}$, to account for the angle of incidence θ_{inc} between $\mathbf{p}$ and the Earth surface.

When the values of the projected antenna pattern are computed in all the points of the integration grid, it is finally re-normalized to the appropriate value above the threshold (as defined in Sec. 4.7.3).

5.5.3. Gaussian_projected and Instrument (SMAP)

The projection algorithms require some modification for SMAP due to some missing information in the L1b data. In particular, the attitude matrix and the feedhorn offset are not provided. Moreover, satellite position and velocities are only provided once per scan as an average value across the scan. The attitude matrix can be computed from the components in the ECEF frame of the satellite position and the satellite velocity. Assuming the radiometer mirror's rotation axis is exactly nadir-aligned (passing through Earth's center), the attitude matrix is then the rotation matrix from the satellite body frame to the ECEF frame.
The feedhorn offset can, in principle, be inferred by computing the difference between

(1) the coordinates on Earth (longitude, latitude) of the L1b data point and

(2) the intersection of the boresight with the Earth's surface by assuming that no feedhorn offset is present.

Unfortunately, the unique angles (θ_{off}, ϕ_{off}) representing the feedhorn offset for each measurement could not be found. Since the ATBD and data product documents of SMAP do not provide an explanation for this, a different approach is followed: whenever projecting the antenna pattern relative to a measurement, the projection is shifted by ($\Delta\mathrm{lon}, \Delta\mathrm{lat}$) on the Earth's surface so that

the boresight intersection with the Earth surface coincides with the coordinates of the measurement from the L1b data.

5.6. Target Antenna Pattern for L1r and L1c Regridding

Interpolation algorithms requiring antenna pattern projection (BG, rSIR, CG, LW) always take as input:

- Source antenna patterns, i.e., the antenna patterns corresponding to the input L1b measurements.

- A target antenna pattern, i.e., the antenna pattern corresponding to the point where the interpolated value needs to be computed.

This is true both for L1r and L1c regridding, with the only difference being the choice of the target antenna pattern (functional form and projection method).

For L1r regridding, the three methods outlined above for the projection of the antenna patterns are chosen by the user for the source and the target antenna pattern separately.

For L1c regridding, the target antenna pattern is designed to represent a cell of the output grid. So, its projection method is always “gaussian” with zero rotation and standard deviation $\sigma_x = \sigma_y$ equal to the size of the output cell. For map projection methods featuring cells with irregular shapes, the size is approximated to the square root of the cell area.